

Interchange of Weyl points in the phonon bands of a half-metal alloy

Stephen J. Jenkins ^{1,*} and G. P. Srivastava ²

¹*Yusuf Hamied Department of Chemistry, University of Cambridge, Lensfield Road, Cambridge CB2 1EW, United Kingdom*

²*Department of Physics and Astronomy, University of Exeter, Stocker Road, Exeter EX4 4QL, United Kingdom*



(Received 9 October 2023; accepted 30 January 2024; published 26 February 2024)

We demonstrate that the topological charge associated with nontrivial phononic Weyl points may be interchanged between nonadjacent locations within the Brillouin zone of a strained crystal. This occurs in our NiMnSb test case upon passing between tensile and compressive uniaxial strain through the higher-symmetry unstrained geometry, and compensates for what would otherwise appear to be nonconservation of topological charge. The phenomenon is dictated by the material's crystallographic point group, and should be replicated in other crystals of similar symmetry.

DOI: [10.1103/PhysRevB.109.085140](https://doi.org/10.1103/PhysRevB.109.085140)

I. INTRODUCTION

In both electronic and vibrational band structures of bulk crystals, twofold band crossings have garnered much attention over recent years [1,2]. These may arise through a simple coincidence of symmetry, in which case their degeneracy may be lifted by a suitably asymmetric deformation of the crystal, but are sometimes associated with nontrivial topology that renders them robust against asymmetric strain. Such Weyl points (WPs), as these robust crossings are known, can be characterized by a nonzero integer topological charge that is conserved as the crystal is deformed. When multiple WPs merge, their individual topological charges are summed, but otherwise ought never to vary. Here, we reveal an apparent exception that arises when the topological charges of two nonadjacent WPs are interchanged upon deforming the crystal through a structure with higher symmetry. To exemplify this, we focus upon the vibrational band structure of an archetypal semi-Heusler alloy, namely NiMnSb.

Among the semi-Heusler compounds, several possess half-metallic electronic band structures, meaning that the bands of one spin species cross the Fermi level while those of the opposite do not. In principle, such materials could function as perfect spin valves, naturally supporting the transport of only one spin species through the crystal. In practice, phonon and magnon excitations may well preclude half-metallicity even at temperatures far below the ferromagnetic/paramagnetic transition [3], but in a cryogenic context the ideal behavior remains an attractive proposition. NiMnSb, crystallizing in the $C1_b$ structure [4], was the first predicted half-metal [5], and has been studied with some regularity over several decades

[6,7]. One of us has published previously on the surface properties of this material, noting the existence of Dirac cones in bands associated with surface-localized minority-spin electronic states that may themselves present a further impediment to the realization of functional devices based upon bulk half-metallicity [8–10]. In the present paper, however, we discuss instead the vibrational band structure of the bulk crystal, emphasizing the influence of uniaxial strain.

II. METHODOLOGY

First-principles density functional theory (DFT) calculations were carried out using the CASTEP computer code (version 18.1) [11]. Electronic wave functions were expanded in a basis set of plane waves, up to a kinetic energy cutoff at 700 eV, and exchange-correlation interactions were incorporated via the Perdew-Becke-Ernzerhof (PBE) functional [12]. Electron-ion interactions were included through the use of ultrasoft pseudopotentials [13] generated using CASTEP's default settings, with nominal valence configurations of $[3d^8, 4s^2]$ for Ni, $[3s^2, 3p^6, 3d^5, 4s^2]$ for Mn, and $[4d^{10}, 5s^2, 5p^3]$ for Sb.

Initial optimization of unstrained NiMnSb was achieved using its highest-symmetry primitive unit cell (spanned by face-centered-cubic primitive lattice vectors) with the Brillouin zone sampled on a Monkhorst-Pack [14] mesh of dimension $8 \times 8 \times 8$. A theoretical cubic lattice constant of 5.916 Å was obtained, converged to within a stress tolerance of 10^{-1} GPa and a change in total energy of no more than 2×10^{-5} eV per atom from one geometry-search iteration to the next.

To provide a reference for later uniaxially strained calculations, we also confirmed that comparable results would be obtained when representing the unstrained structure using the smallest conventional body-centered-tetragonal cell, sampled on a mesh of dimension $8 \times 8 \times 6$. This approach gave rise to a theoretical lattice constant differing from the previous value only in the seventh significant figure. Similarly, we also tested the use of a conventional cubic cell (Fig. 1) sampled on a mesh of dimension $6 \times 6 \times 6$, obtaining a theoretical lattice

*sjj24@cam.ac.uk

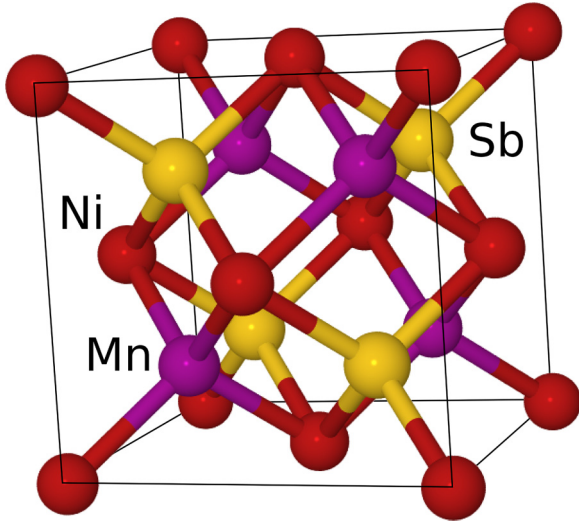


FIG. 1. Conventional unit cell of NiMnSb, four times the volume of its primitive unit cell. The material has a face-centered-cubic (fcc) real-space lattice with a basis comprising Ni:(0.00,0.00,0.00), Mn:(0.25,0.25,0.25), Sb:(0.75,0.75,0.75).

constant indistinguishable from the first to eight significant figures. Clearly the numerical errors associated with differing cell geometry and \mathbf{k} -point sampling are very small indeed for this system while using the stated parameters.

For ease of applying suitable constraints to the strained geometries studied here, free lattice parameters in each case were initially optimized within conventional unit cells prior to conversion to primitive unit cells. For instance, when considering a 1% uniaxial stretch, we first set up a conventional body-centered-tetragonal cell containing two NiMnSb structural units (i.e., six atoms in all) and increased the long side to a length of 5.975 Å. Fixing the latter value, the short sides of the cell relaxed to an optimal length of 4.170 Å. Results from other uniaxially strained geometries are presented in Table I.

Knowing these various lattice constants, it was then possible to characterize fully the real-space and reciprocal lattices of the strained systems, and hence to determine the exact size and shape of the strained Brillouin zones, following

TABLE I. Side lengths of conventional body-centered-tetragonal unit cells used in the present work for constrained structural optimization. With the long side set to $c = 5.916$ Å and the short sides to $a = 4.183$ Å, the structure is equivalent to face-centered-cubic with a lattice parameter equal to a . In all other cases, the long side has been set to a fixed percentage strain and the short sides allowed to relax.

Δc	a (Å)	c (Å)
-1.0%	4.194	5.857
-0.1%	4.185	5.910
$\pm 0.0\%$	4.183	5.916
+0.1%	4.182	5.922
+0.5%	4.177	5.946
+1.0%	4.170	5.975
+1.5%	4.164	6.005
+2.0%	4.154	6.035

TABLE II. Lengths and angular separations of real-space lattice vectors spanning primitive unit cells corresponding to the conventional unit cells described in Table I.

Δc	$ \mathbf{a}_n $	θ_{12}	$\theta_{23} = \theta_{31}$
-1.0%	4.168	90.721°	119.585°
-0.1%	4.182	90.076°	119.956°
$\pm 0.0\%$	4.183	90.000°	120.000°
+0.1%	4.185	89.921°	120.046°
+0.5%	4.191	89.620°	120.219°
+1.0%	4.198	89.244°	120.437°
+1.5%	4.205	88.874°	120.652°
+2.0%	4.211	88.457°	120.895°

conventions systematically laid out by Setyawan and Curtarolo [15]. The lengths of three primitive real-space lattice vectors, \mathbf{a}_1 , \mathbf{a}_2 , and \mathbf{a}_3 , are provided in Table II, along with the angles between them, θ_{12} , θ_{23} , and θ_{31} . Equivalent information for reciprocal lattice vectors \mathbf{b}_1 , \mathbf{b}_2 , and \mathbf{b}_3 , and for their angles, ϕ_{12} , ϕ_{23} , and ϕ_{31} , may be found in Table III. These are the geometric parameters with respect to which we report coordinates of band crossings in the Supplemental Material (SM) [16].

Calculations of dynamical matrices were carried out within tetragonally strained near-cubic supercells (all side lengths being approximately 11.832 Å) containing 32 NiMnSb structural units, using a Monkhorst-Pack mesh of dimension $2 \times 2 \times 2$. Prompted by comments in a recent publication from Kendrick and Burnett [17] we not only set the real-space integration “grid_scale” parameter to a value of 2.0, but also set the “fine_grid_scale” parameter to 6.0, to ensure adequate representation of low-frequency acoustic modes. Convergence criteria for the electronic structure were set at 10^{-11} eV for the total energy, 10^{-13} eV for individual eigenvalues, and 10^{-5} eV Å $^{-1}$ for the calculated forces. Only with all three criteria satisfied would the resulting structures be used for the computation of vibrational properties.

Topological analysis of the calculated vibrational band structures was performed by evaluating the Berry phase [18] via the Wilson loop [19] method (see SM [16] for technical details). The Berry phase for an isolated band must be an integer multiple of 2π , but in the vicinity of a WP the Berry phases of its two crossing bands may interchange smoothly,

TABLE III. Lengths and angular separations of primitive reciprocal lattice vectors derived from the real-space lattice vectors defined in Table II. Coordinates listed in the SM [16] are expressed as fractions of these basis vectors.

Δc	$ \mathbf{b}_1 = \mathbf{b}_2 $	$ \mathbf{b}_3 $	ϕ_{12}	$\phi_{23} = \phi_{31}$
-1.0%	1.843	2.119	70.187°	54.906°
-0.1%	1.840	2.123	70.493°	54.754°
$\pm 0.0\%$	1.839	2.124	70.529°	54.736°
+0.1%	1.839	2.125	70.566°	54.717°
+0.5%	1.838	2.128	70.707°	54.646°
+1.0%	1.837	2.131	70.883°	54.558°
+1.5%	1.836	2.134	71.055°	54.472°
+2.0%	1.836	2.139	71.248°	54.376°

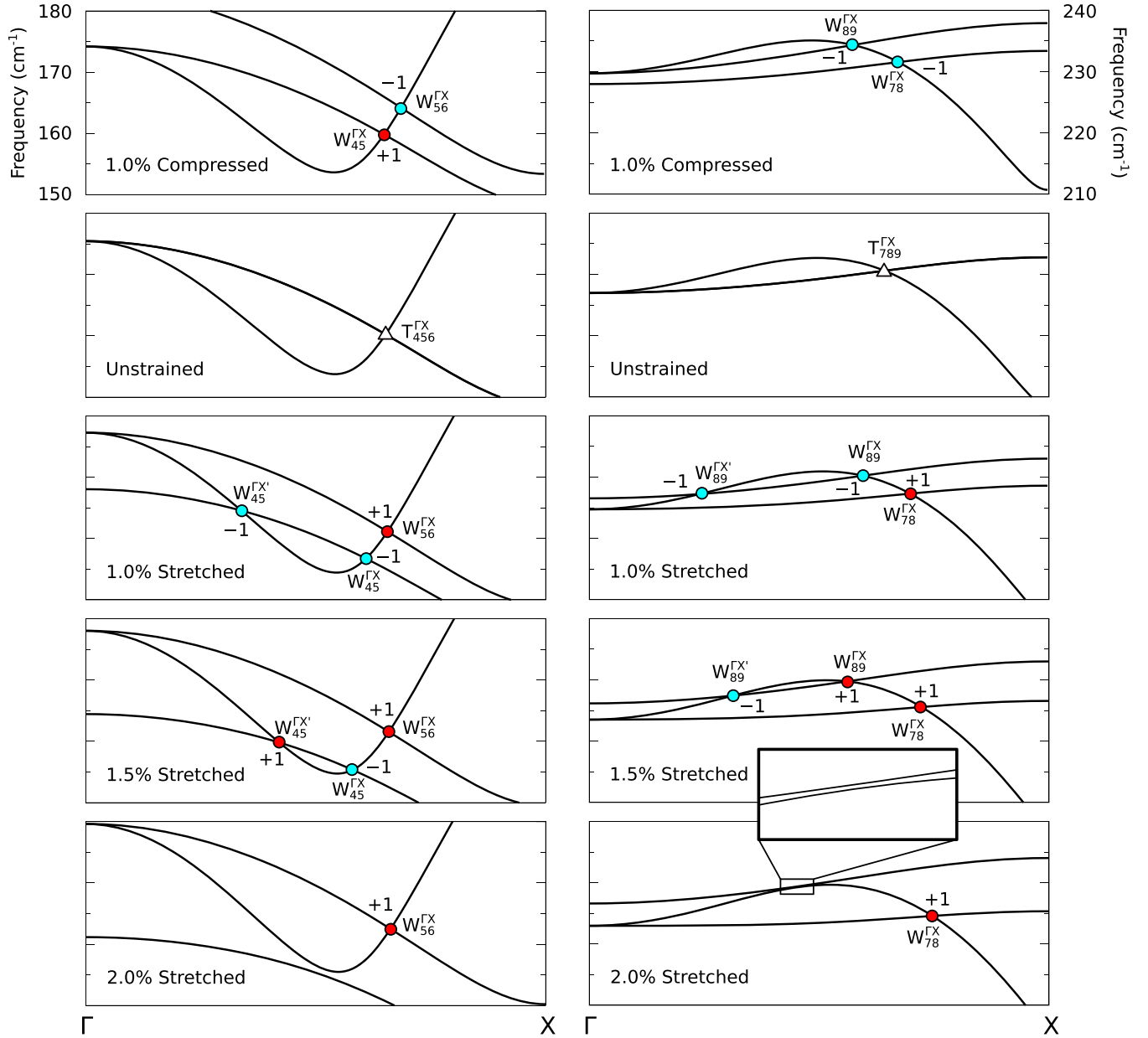


FIG. 3. Influence of uniaxial [001] strain on bands 4, 5, and 6 (left panels) and on bands 7, 8, and 9 (right panels) along the Γ -X direction. WPs with positive and negative topological charges are indicated by red and cyan circles; TDNPs are marked with white triangles.

the resulting net charge in each case is zero and the associated crossing no longer topologically protected. With the tensile strain increased to 2.0%, therefore, the only remaining on-axis WPs are $W_{56}^{\Gamma X}$ and $W_{78}^{\Gamma X}$, both carrying a topological charge of +1, the others having annihilated in pairwise fashion. The mystery, of course, is how the topological charges of $W_{45}^{\Gamma X'}$ and $W_{89}^{\Gamma X}$ change sign, given our expectation of charge conservation.

Fortunately, the answer to this conundrum is relatively simple. Investigation of regions lying off the Γ -X axis reveals a pair of positively charged WPs converging upon $W_{45}^{\Gamma X'}$ (and another pair converging upon $W_{89}^{\Gamma X}$) as the tensile strain is increased from 0.1%, through 0.5%, to 1.0%. Under strain approaching 1.5%, these pairs of WPs have simply merged with the on-axis WPs to create an apparent change in sign

of the associated topological charge. A similar merger with two countercharged WPs almost certainly accounts for the apparent change in sign of $W_{89}^{\Gamma X}$ upon reducing compressive strain from 0.5% to 0.1%, as briefly alluded to above. Taking the bigger picture into account, topological charge is actually conserved precisely as expected in all of these cases.

Before returning to the WPs of the unstrained system, it may be wise to review the role of symmetry in dictating the relationship between WPs at different locations within the Brillouin zone. We begin by noting the importance of the crystallographic point group formed from the space group of the crystal by converting glide and screw operations into reflection and rotation operations respectively. The space group of unstrained NiMnSb is $F43m$ and its point group $43m$.

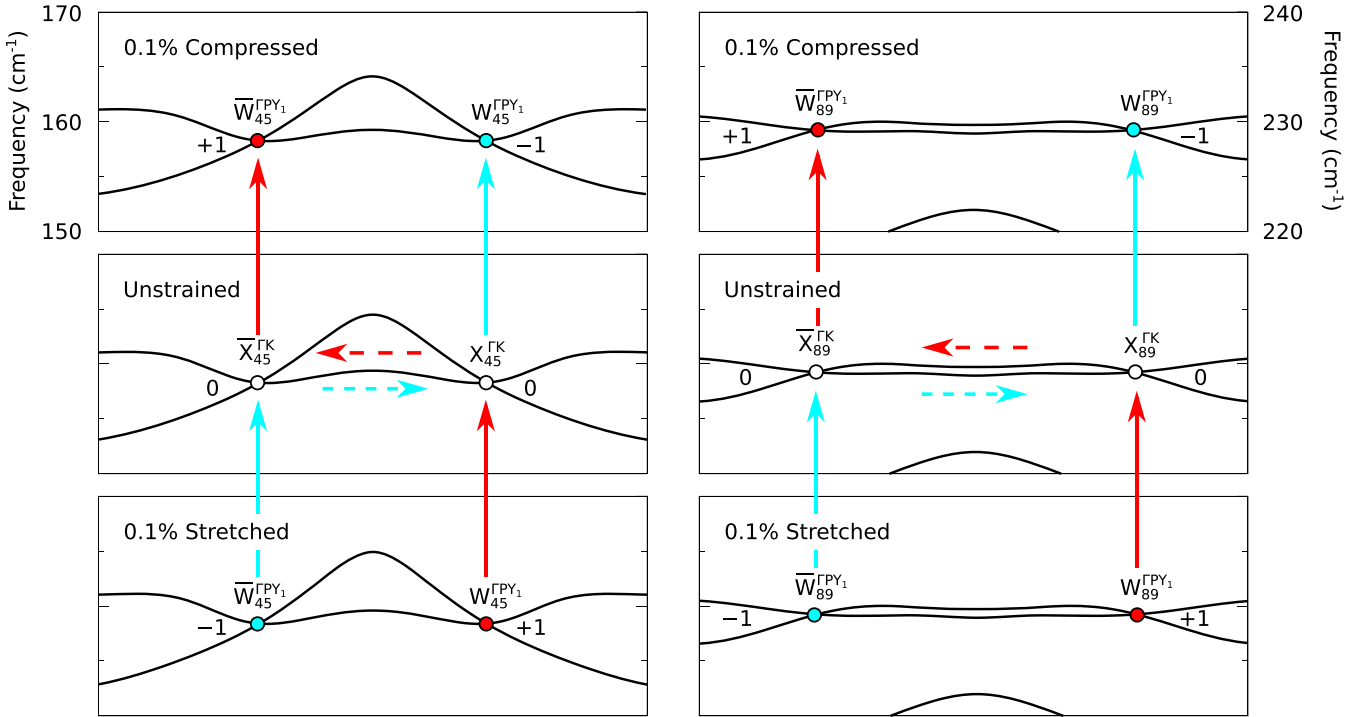


FIG. 4. Influence of uniaxial [001] strain on a band crossing and its mirror image, both formed by bands 4 and 5 (left panels) and by bands 8 and 9 (right panels). Details of the precise path taken through reciprocal space are provided in the SM [16]. Positive and negative topological charges are indicated by red and cyan circles; white circles are uncharged.

When uniaxially strained in the [001] direction, the space group reduces to $I4m2$, with point group $\bar{4}2m$.

Let us proceed by denoting the mean atomic positions in our system as \mathbf{R}_m , where m is simply a numerical index. Taking $\hat{\sigma}$ to be an operation within the crystallographic point group, its action upon \mathbf{R}_m must amount to a mere reindexing among the same set of positions. Then, letting $\epsilon_n(\mathbf{q})$ represent the vibrational eigenfrequency of mode n at wave vector \mathbf{q} , with $\mathbf{u}_n(\mathbf{q}, \mathbf{R}_m)$ being the corresponding displacement amplitude for the atom that oscillates around \mathbf{R}_m , it follows that $\epsilon_n(\hat{\sigma}\mathbf{q}) = \epsilon_n(\mathbf{q})$ and that $\mathbf{u}_n(\hat{\sigma}\mathbf{q}, \mathbf{R}_m) = \hat{\sigma}\mathbf{u}_n(\mathbf{q}, \hat{\sigma}^{-1}\mathbf{R}_m)$. Additionally, time-reversal symmetry allows us to state that $\epsilon_n(-\mathbf{q}) = \epsilon_n(\mathbf{q})$ and that $\mathbf{u}_n(-\mathbf{q}, \mathbf{R}_m) = \mathbf{u}_n^*(\mathbf{q}, \mathbf{R}_m)$ in all cases.

Given these relationships, it further follows that if the locations of two band crossings are related via a proper symmetry operation of the point group (identity or rotation) then they must share the same topological charge, while if they are related via an improper symmetry operation of the point group (reflection or inversion) then they must have topological charges of equal magnitude but opposite sign. One corollary of this is that true WPs (having nonzero topological charge) are possible only when the point group lacks inversion symmetry. A second is that any band crossing lying on a mirror plane of the point group must necessarily be topologically trivial, since it is related to itself both by a proper operation (identity) and by an improper operation (reflection). In the present context, this means we could have predicted that the six band crossings lying on high-symmetry directions of the unstrained system would all turn out to be topologically trivial since all do, indeed, lie upon mirror planes of the point

group. Our calculations, in this respect, merely bear out this necessary fact.

Nevertheless, despite this unpromising conclusion, we find that the two crossings denoted $W_{45}^{\Gamma PY_1}$ and $W_{89}^{\Gamma PY_1}$ (identifiers for $X_{45}^{\Gamma K}$ and $X_{89}^{\Gamma K}$ adapted for the irreducible zones of the strained systems) are actually robust upon the application of tensile strain. Furthermore, in the 0.1% stretched case, both are found to acquire a topological charge of +1, justifying our labeling them with an initial W (Figs. 4 and 5). In the strained system, however, they no longer lie on a high-symmetry direction, and so are free to migrate within the Γ - P - Y_1 plane as the strain is increased. In fact, the pair of WPs comprising $W_{45}^{\Gamma PY_1}$ and its image formed by twofold rotation about the Γ - X axis turns out to be the very same pair responsible for the apparent change in sign of $W_{45}^{\Gamma X}$ noted above as tensile strain is increased from 1.0% to 1.5%. The approximately concurrent change in sign of $W_{89}^{\Gamma X}$, on the other hand, is accounted for by the positively charged WP labeled $W_{89}^{\Gamma PX}$ (and its similarly rotated image)—previously denoted $W_{89}^{\Gamma WX}$ within the unstrained system.

Already, however, the situation appears problematic. How can $W_{45}^{\Gamma PY_1}$ and $W_{89}^{\Gamma PY_1}$ carry nonzero topological charges in the strained case that vanish when the strain is removed? Such an observation appears to be at odds with our expectation that topological charge must be conserved, and on this occasion there are no additional WPs to be found in the vicinity that could account for the discrepancy. What is missing from this picture, of course, is the additional symmetry that pertains to the unstrained case. Specifically, for each WP within the irreducible segment of the strained Brillouin zone, an image exists elsewhere within the full Brillouin zone that carries

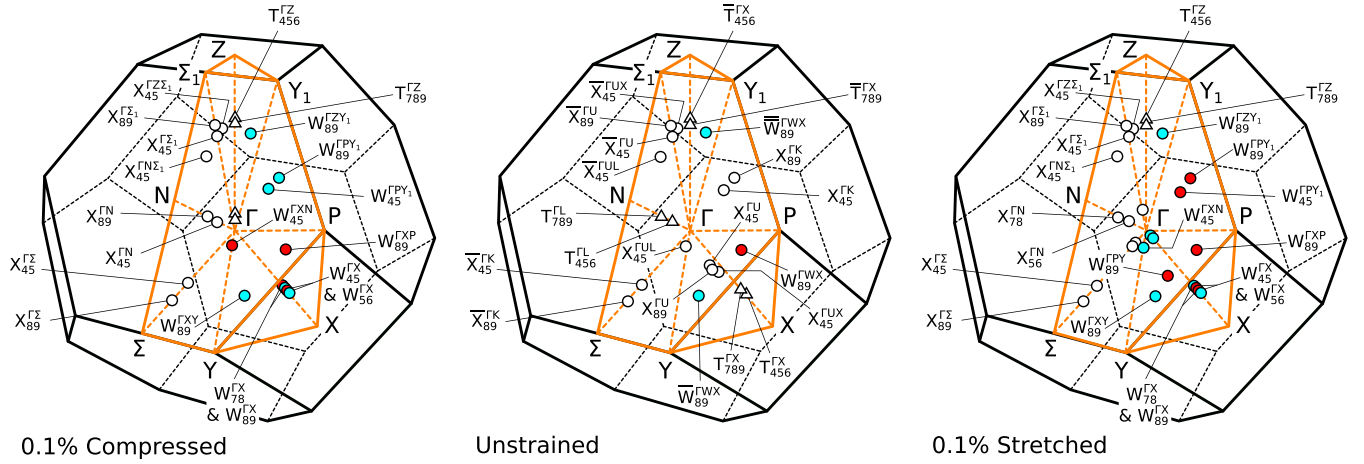


FIG. 5. Locations of twofold (circles) and threefold (triangles) band crossings for NiMnSb in its unstrained geometry and under conditions of 0.1% compressive or tensile strain along [001] (i.e., the Γ -Z direction). All are shown within the irreducible segment consistent with the strained cases [15]. Red and cyan shadings indicate positive and negative topological charge, respectively, while unshaded points are uncharged.

the opposite charge, lying at a position related by mirror symmetry to its partner (denoted with an overline in Fig. 4). In the unstrained case, however, the original WP and its image are also linked by threefold rotational symmetry, so that they become indistinguishable and collapse to a trivial band crossing. The change in apparent topological charge from nonzero to zero is, indeed, due to the presence of a second WP, albeit one that lies distant from the first. But what might one predict about the topological charge as each WP passes through its zero-charge unstrained instance and transforms into the version consistent with compressive strain? Will its topological charge revert to the same value as for the tensile case, or might something more surprising happen?

In fact, our calculations under 0.1% compressive strain indicate topological charges for $W_{45}^{\Gamma PY_1}$ and $W_{89}^{\Gamma PY_1}$ of -1 . Their individual topological charges reverse sign, therefore, when passing from the stretched to the compressed case, as if WPs of opposing charge have interchanged their locations within the Brillouin zone. Topological charge continues to be conserved, but only if we accept that WPs can, in effect, “teleport” (i.e., travel without passing through intermediate locations) from one irreducible segment of the Brillouin zone to another when the system passes through a high-symmetry intermediate structure. That this can be reconciled with the symmetry of our system may be demonstrated as follows.

Starting with the unstrained system, consider the effect of uniaxial strain along a general axis \mathbf{s} causing an uncharged band crossing located at some point \mathbf{q} to acquire a certain topological charge. If the strain were instead applied along an axis $\hat{\sigma}\mathbf{s}$, then an equivalent band crossing located at $\hat{\sigma}\mathbf{q}$ would acquire either the same topological charge (if $\hat{\sigma}$ is a proper operation) or the opposite (if $\hat{\sigma}$ is improper). Combining the reflection and threefold rotation symmetries of the $\bar{4}3m$ point group, one may demonstrate that the topological charges associated with $W_{45}^{\Gamma PY_1}$ and $W_{89}^{\Gamma PY_1}$ under the imposition of compressive strain along the [001] axis must be opposite to the topological charges associated with the same WPs under the imposition of compressive strain along the [010] axis. It is, however, possible to continuously deform the system

from the latter condition into one of tensile strain applied along the [001] axis, passing through a series of intermediate orthorhombic geometries. Since this does not involve passing through any higher-symmetry structures, it follows that $W_{45}^{\Gamma PY_1}$ and $W_{89}^{\Gamma PY_1}$ cannot change their signs while we do so. Accordingly, we have demonstrated through symmetry alone that the topological charges of these particular WPs while under tensile strain along [001] must be equal and opposite to their charges under compressive strain along the same axis.

An exactly similar argument may now be applied to the WP labeled $W_{45}^{\Gamma XN}$, which carries a charge of $+1$ under compressive strain and of -1 under tensile strain, passing through an uncharged condition ($X_{45}^{\Gamma UL}$) in the unstrained case. Conversely, the crossing denoted $X_{45}^{\Gamma U}$ in the unstrained system is simply not robust under either compressive or tensile strain, while that labeled $X_{89}^{\Gamma U}$ acquires a charge of $+1$ when relabeled $W_{89}^{\Gamma PY}$ under tensile strain but annihilates with a mirror image when crossing over to the compressed scenario. Both behaviors are again entirely consistent with the respective symmetries of the strained and unstrained crystals. Finally, note that the charge on $W_{89}^{\Gamma XP}$ (the relabeled counterpart of unstrained $W_{89}^{\Gamma WX}$) is conserved throughout, because it does not pass through a higher-symmetry condition in moving between tensile and compressive conditions.

IV. CONCLUSIONS

In summary, we have investigated the topology of twofold crossings within the vibrational band structure of NiMnSb, showing that imposition of strain along [001] causes two uncharged TDNPs to split into pairs of nontrivial WPs. We describe four further band crossings that carry no topological charge in the unstrained case but that acquire nonzero topological charge (becoming true WPs) in certain strained cases, demonstrating that these topological charges change sign in switching between tensile and compressive strain. In effect, these WPs teleport from one irreducible segment of the Brillouin zone to another when passing through the unstrained

case, explaining both the interchange of sign and intermediate cancellation of topological charge. Where a true WP is already present in the unstrained case, however, no teleportation is possible and its charge must straightforwardly be conserved. Such behaviors are implied by the point group of the unstrained crystal, and should be apparent in the vibrational and/or electronic topologies of other systems having similar symmetry.

Computer code and data supporting this paper are openly available from Apollo, the University of Cambridge data repository [21].

ACKNOWLEDGMENT

Computational resources were provided by the Cambridge Service for Data-Driven Discovery (CSD3).

-
- [1] J. Li, Q. Xie, S. Ullah, R. Li, H. Ma, D. Li, Y. Li, and X.-Q. Chen, Coexistent three-component and two-component Weyl phonons in TiS, ZrSe, and HfTe, *Phys. Rev. B* **97**, 054305 (2018).
- [2] Q. Xie, J. Li, S. Ullah, R. Li, L. Wang, D. Li, Y. Li, S. Yunoki, and X.-Q. Chen, Phononic Weyl points and one-way topologically protected nontrivial phononic surface arc states in noncentrosymmetric WC-type materials, *Phys. Rev. B* **99**, 174306 (2019).
- [3] C. N. Borca, D. Ristoiu, H.-K. Jeong, T. Komesu, A. N. Caruso, J. Pierre, L. Ranno, J. P. Nozieres, and P. A. Dowben, Epitaxial growth and surface properties of half-metal NiMnSb films, *J. Phys.: Condens. Matter* **19**, 315211 (2007).
- [4] L. Wollmann, A. K. Nayak, S. S. P. Parkin, and C. Felser, Heusler 4.0: Tunable materials, *Annu. Rev. Mater. Res.* **47**, 247 (2017).
- [5] R. A. de Groot, F. M. Mueller, P. G. van Engen, and K. H. J. Buschow, New class of materials: Half-metallic ferromagnets, *Phys. Rev. Lett.* **50**, 2024 (1983).
- [6] C. N. Borca, T. Komesu, H.-K. Jeong, P. A. Dowben, D. Ristoiu, C. Hordequin, J. Pierre, and J. P. Nozieres, Effective surface Debye temperature for NiMnSb(100) epitaxial films, *Appl. Phys. Lett.* **77**, 88 (2000).
- [7] J. J. Attema, G. A. de Wijs, and R. A. de Groot, Optimizing performance of half-metals at finite temperature, *J. Phys.: Condens. Matter* **19**, 315212 (2007).
- [8] S. J. Jenkins and D. A. King, Minority metallic surface states of a half-metallic ferrimagnet, *Surf. Sci.* **494**, L793 (2001).
- [9] J. P. Velev, P. A. Dowben, E. Y. Tsymlal, S. J. Jenkins, and A. N. Caruso, Interface effects in spin-polarised metal/insulator layered structures, *Surf. Sci. Rep.* **63**, 400 (2008).
- [10] S. J. Jenkins, Tilted elliptical Dirac cones at a half-metal surface, *Phys. Rev. B* **82**, 020403(R) (2010).
- [11] S. J. Clarke, M. D. Segall, C. J. Pickard, P. J. Hasnip, M. J. Probert, K. Refson, and M. C. Payne, First-principles methods using CASTEP, *Z. Kristallogr.* **220**, 567 (2005).
- [12] J. P. Perdew, K. Burke, and M. Ernzerhof, Generalized gradient approximation made simple, *Phys. Rev. Lett.* **77**, 3865 (1996).
- [13] D. Vanderbilt, Soft self-consistent pseudopotentials in a generalized eigenvalue formalism, *Phys. Rev. B* **41**, 7892 (1990).
- [14] H. J. Monkhorst and J. D. Pack, Special points for Brillouin-zone integrations, *Phys. Rev. B* **13**, 5188 (1976).
- [15] W. Setyawan and S. Curtarolo, High-throughput electronic band structure calculations: Challenges and tools, *Comput. Mater. Sci.* **49**, 299 (2010).
- [16] See Supplemental Material at <http://link.aps.org/supplemental/10.1103/PhysRevB.109.085140> for methodological details and comprehensive tabulation of band crossing data.
- [17] J. Kendrick and A. D. Burnett, Exploring the reliability of DFT calculations of the infrared and terahertz spectra of sodium peroxodisulfate, *J. Infrared Millim. Terahertz Waves* **41**, 382 (2020).
- [18] M. V. Berry, Quantal phase factors accompanying adiabatic changes, *Proc. R. Soc. London, Ser. A* **392**, 45 (1984).
- [19] K. G. Wilson, Confinement of quarks, *Phys. Rev. D* **10**, 2445 (1974).
- [20] Z. Zhu, G. W. Winkler, Q. S. Wu, J. Li, and A. A. Soluyanov, Triple point topological metals, *Phys. Rev. X* **6**, 031003 (2016).
- [21] Apollo, University of Cambridge data repository, doi:10.17863/CAM.105656 (for computer code) and doi:10.17863/CAM.105658 (for data).